Indian J Microbiol (Oct–Dec 2021) 61(4):487–496
https://doi.org/10.1007/s12088-021-00973-z

ORIGINAL RESEARCH ARTICLE

Photocatalytic TiO_2/CdS/ZnS nanocomposite induces *Bacillus subtilis* cell death by disrupting its metabolism and membrane integrity

Naveen Kumar[1] · Anuj Mittal[1] · Monika Yadav[2] · Shankar Sharma[1] · Tarun Kumar[2] · Rahul Chakraborty[3] · Shantanu Sengupta[3] · Nar Singh Chauhan[2]

Received: 24 July 2021 / Accepted: 8 August 2021 / Published online: 18 August 2021

Abstract Titanium dioxide (TiO_2) is widely characterized for its application in clinical diagnostics, therapeutics, cosmetics, nutrition, and environment management. Despite enormous potential, its dependence on ultraviolet (UV) light for photocatalytic activity limits its commercialization. Accordingly in the present study, a photo catalytically superior ternary complex of TiO_2 with Cadmium sulfide/Zinc sulfide (CdS/ZnS) has been synthesized, as well as, characterized for photo-induced antimicrobial activity. The band gap of crystalline TiO_2/CdS/ZnS nanocomposite has been reduced (2.26 eV) and nanocomposite has shown the optimal photo-activation at 590 nm. TiO_2 nanocomposite has significant bactericidal activity in visible light ($P < 0.01$). Exposure of the TiO_2 nanocomposite affected the cellular metabolism by altering the 1681 metabolic features ($P < 0.001$) culminating in poor cellular survivability. Additionally, photo-induced reactive oxygen species generation through nanocomposite disrupts the microbial cellular structure. The present study synthesized photocatalytic nanocomposite as well as unveiled the holistic cellular effect of theTiO_2/CdS/ZnS nanocomposite. Additionally, the present study also indicated the potential application of TiO_2/CdS/ZnS nanocomposite for sustainable environment management, therapeutics, and various industries.

✉ Nar Singh Chauhan
nschauhan@mdurohtak.ac.in

[1] Department of Chemistry, Maharshi Dayanand University, Rohtak, Haryana, India

[2] Department of Biochemistry, Maharshi Dayanand University, Rohtak, Haryana, India

[3] Council of Scientific and Industrial Research-Institute of Genomics and Integrative Biology, New Delhi, India

Keywords TiO_2 nanocomposite · TiO_2 bioactivity · Photocatalysis · Photoactivity · Reactive oxygen species · Metabolomics

Introduction

In the past few decades, the biotechnological sectors are playing a significant role in sustainable development. Multidisciplinary approaches have been employed for efficient biocatalysts and biotransformation processes [1–7]. Engineering of bioprocess and biocatalysts are largely used to improve the production of biomolecules [8–11]. Particularly, the nanotechnology sector is gaining a vital role in developing nano-biocatalyst for various biotechnological applications due to their unique features [12–16]. Multiple materials, bioactive molecules, and microbes have been widely used as therapeutic, antimicrobials, or pathogen inhibition applications [17–22]. Due to higher selectivity and specificity, nanomaterials are more beneficial for antimicrobials' purposes than others [23, 24].

Titanium dioxide nanoparticles were characterized for their potential in a wide range of industrial applications [25]. Photo-excitation of TiO_2 nanoparticles generates reactive oxygen species that could potentially kill microbes and degrade organic pollutants, industrial dyes, etc. These properties augmented its application potential in the area of therapeutics and environment management [25]. TiO_2 has a bandgap between 3.0 and 3.2 eV that allows electron excitation only in the UV range of the electromagnetic spectrum. Limited visible light absorption does not allow its photo-activation to achieve the desired photo-catalytic properties, limiting its augmentation for industrial applications [26]. Efforts are being made for TiO_2 bandgap

engineering through various extrinsic modifications. It includes doping with metal and non-metals, developing metal oxide nanoconjugates, etc. [27]. In this trend, our previous report showed TiO_2/CdS/ZnS photocatalyst with varied concentrations of CdS and ZnS that absorbs up to 590 nm and shifts the band from 3.18 eV in TiO_2 to 2.26 eV in TiO_2/CdS (20%)/ZnS (10%) [28]. This composition showed optimal photocatalytic activity for the degradation of an organic moiety. An optimal nanomaterial for industrial, environmental, and therapeutic applications should be stable, self-sustainable, inexpensive, and should possess bactericidal properties [23, 24]. The antimicrobial activity of TiO_2 nanoparticles has been reported in recent studies [29]. TiO_2 nanoparticles induce antimicrobial activity either by altering microbial cell physiology [29] or through Reactive Oxygen Species (ROS)-induced microbial cell rupture [30]. These studies were performed in isolation, and no significant effort was made to report the holistic mechanism of action of the nanoparticles as antimicrobial agents. The antimicrobial property of the photocatalytic nanocomposite needs to be assessed by exploring their effect on the microbial cell structure and metabolism [23, 24, 29, 30]. The current study was designed with two broader objectives: the synthesis of photocatalytic nanocomposite and the exploration of their holistic mechanism of antimicrobial action.

Materials and Methods

Materials

The reagents titanium isopropoxide, cadmium sulfate ($3CdSO_4.8H_2O$), thiourea, and zinc nitrate were supplied by Sigma Aldrich. The sodium sulfide was purchased from Central Drug House (CDH) Ltd (India). Analytical grade chemicals were used without purification for the future process.

Synthesis and Characterization of TiO_2/CdS/ZnS Nanocomposites

The synthesis of TiO_2/CdS/ZnS ternary nanocomposite was done using the hydrothermal approach described in our earlier report [28]. The crystallinity and phase of the nanocomposite were analyzed using Rigaku Ultima IV powder X-ray diffractometer in the 2θ range of 20° to 80°. UV–visible diffuse reflectance spectrophotometer (Shimadzu 3600 Plus) was used to determine the optical characteristics. A Field Emission Scanning Electron Microscope determined the morphology of the synthesized sample (FESEM) operated at 30 kV. Transmission Electron Microscope (TEM) (Tecnai G2 20) operated at 200 kV was used to determine the particle size of the nanocomposite.

Antimicrobial Activity

The antimicrobial activity of nanoparticles was assessed against *Bacillus subtilis* (MTCC No. 2057) with standard approaches like disc diffusion assay and Micro broth dilution assay (Supplementary method SM1). All the experiments were performed in biological triplicates.

Estimation of Reactive Oxygen Species and Lipid Peroxidation

TiO_2/CdS/ZnS nanocomposite induced cellular generation of reactive oxygen species (ROS) was analyzed [31]. To check the oxidative degradation of bacterial lipids due to nanoparticles, a lipid peroxidation assay was performed [31]. Tests were performed in triplicates.

Analysis of Microbial Cell Morphology

Field Emission Scanning Electron Microscopy (FESEM) of the samples was performed at the central instrumentation facility at NIMS, Jaipur, Rajasthan, India. Untreated microbial cells were used as a control. All the experiments were performed in biological triplicates.

Metabolomic Analysis

The effect of nanocomposite on cellular metabolism was assessed after analyzing whole-cell metabolites with Liquid Chromatography with tandem mass spectrometry (LC–MS) (Supplementary method SM2). LC/MS-based metabolic profiles generated with both negative and positive mode Electrospray Ionization (ESI) were analyzed with XCMS software running under R environment version 3.7.1 for metabolic feature detection, chromatographic matching, and metabolite mapping using *Bacillus subtilis* metabolomic profile as a reference library by following its default settings.

Statistical Analysis

All experiments were carried out in triplicate. Statistical tests were performed to calculate *P*-value, standard deviations, etc.

Results

Characterization of the Synthesized Samples

The X-ray diffraction (XRD) pattern of TiO_2/CdS/ZnS nanocomposite (TCZ-1) shows the major peaks at 2θ 25.38°, 37.86°, 48.15°, 54.13°, 55.21°, and 62.79° that correspond to the anatase phase of TiO_2 and are well-matched with the Joint Committee on Powder Diffraction Standards (JCPDS) card No. 21-127 (Fig. 1a). The peak corresponding to anatase TiO_2 did not show any shift indicating that CdS and ZnS do not affect the basic structure of the lattice. The peaks other than anatase TiO_2 at 2θ 26.53°, 28.53°, 43.91°, and 51.98° indicated the presence of cubic and hexagonal phase of CdS (JCPDS card no. 41-1049), and at 2θ 28.53°, 48.17°, and 56.4° indicated the presence of cubic ZnS(ICDD PDF 65-1691). The peaks corresponding to CdS at 2θ 28.21° and ZnS at 2θ 28.53° superimposed [28]. Debye–Scherrer equation was used to calculate the average crystallite size and found that the size of TiO_2 is about 10 nm while that of CdS and ZnS is

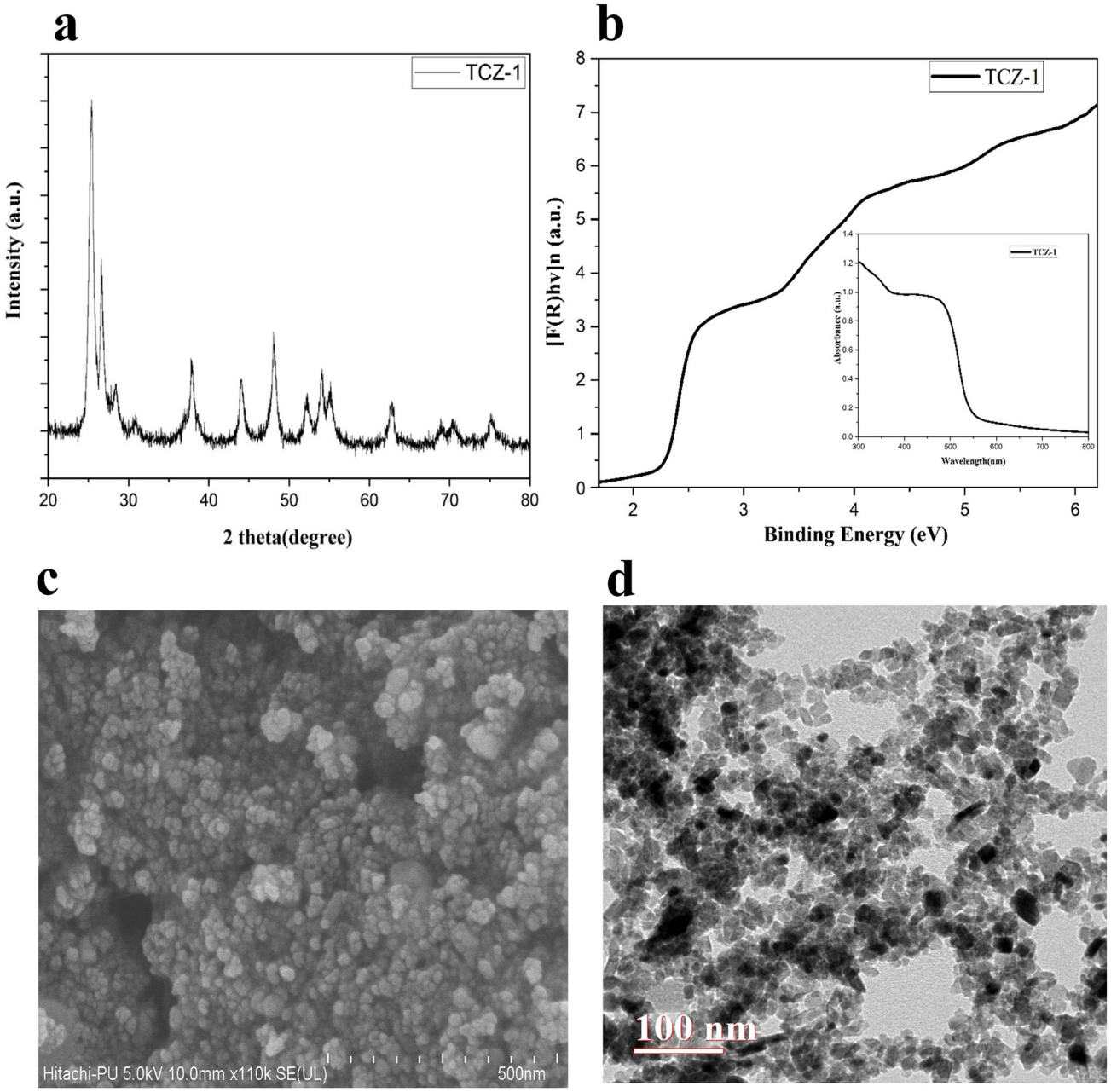

Fig. 1 Characterization of the synthesized sample. TiO_2/CdS/ZnS nanocomposite (TCZ1) was characterized by observing its XRD pattern (**a**) and Kubelkamunk spectra (**b**), FESEM imaging (**c**), and TEM imaging (**d**)

30–40 nm. The optical properties are also studied using a UV visible spectrophotometer (Fig. 1b). The absorbance of the compound over a range of wavelengths is shown (Fig. 1b). The band gap is calculated using the Kubelka–Munk function where reflectance (R) at any wavelength is given as

$$F(R) = \frac{(1-R)^2}{2R}$$

The graph is plotted for indirect bandgap semiconductor materials by taking hν as energy along the x-axis and $[F(R)\ h\nu]^{1/2}$ along the y-axis. It is well known that pure TiO_2 shows absorption in the UV region but it is seen from the spectra that the synthesized compounds showed absorbance near 590 nm corresponding to a bandgap of 2.26 eV. The shift in absorption and lowering of the bandgap is due to the CdS and ZnS in the composite. The enhanced absorption towards the visible region assists the high activity of the composite under visible light exposure. The morphological characteristics were uncovered using FESEM and TEM techniques. The FESEM image of the TCZ-1 sample showed the formation of spherical nanoparticles in the ternary composites (Fig. 1c). The TEM image of the ternary composites shows well-dispersed and uniform particles without any aggregation (Fig. 1d). The particle size estimated from the TEM image is in the nano range and in good agreement with that calculated from the XRD data.

Antimicrobial Activity of the Nanoparticles

Disc diffusion assay indicates antibacterial property against *Bacillus subtilis* (Supplementary Fig. S1). Microbroth dilution assay showed good growth inhibition efficiency of TiO_2/CdS/ZnS towards *Bacillus subtilis*. The minimum inhibitory concentration for *Bacillus subtilis* was 0.1953 mg ml^{-1} in light conditions and 3.125 mg ml^{-1} in dark conditions. Time Kill kinetics assay also indicates an optimum antibacterial activity after incubating the nanoparticle mixture with microbes for 25 min (Supplementary Fig. S2). Bactericidal activity of the nanocomposite was significantly higher ($P < 0.01$) in presence of light as compared to dark conditions (Supplementary Fig. S3).

Mechanism of Antibacterial Activity of Nanocomposite

The average reactive oxygen species (ROS) concentration in nanocomposite treated cells was 471 folds higher than the untreated cells. Even a ~ 273 fold higher membrane lipid oxidation was observed in treated cells compared to untreated cells. Scanning electron micrographs showed adherence of nanocomposite to the microbial cell membrane (Fig. 2a). Changes in the cell morphology, as well as cellular raptures, could easily be observed in the sample treated with nanocomposite (Fig. 2a), while no such changes were observed within control samples (Fig. 2b). Compositional analysis indicates the abundance of nanocomposite elements in treated cells as well as a lower percentage of electrolytes (Supplementary Fig. S4). Nanocomposite-induced cellular changes could be easily monitored by observing the cellular metabolomic profile [32]. It would provide a holistic view of molecular changes induced by external agents [32]. Metabolomic profiling of the nanocomposite treated microbial cell was identified to have 1274 and 407 statistically significant features ($P < 0.01$) after analysis of the metabolic profile captured with positive and negative ESI mode (Fig. 3a and b).

These differentially abundant metabolic features were mapped with metabolic pathways associated with nucleotide metabolism, amino acid metabolism, and membrane precursor synthesis (Tables 1, 2). The metabolic precursors for nucleotide biosynthesis ($P \leq 0.002$), cell wall synthesis ($P \leq 0.002$), protein synthesis ($P \leq 0.0019$), lipid biosynthesis ($P = 0.0019$), pH resistance ($P = 0.00039$), and siderophore formation ($P = 5.9e\text{-}7$) were significantly reduced (Table 1). These results indicate that the introduction of TiO_2/CdS/ZnS nanocomposite arrested the bacterial cell growth by inhibiting electron transport system (by reducing the precursors that mediate the electron transfer by 9.7 folds), vital pathways for protein, lipid, and nucleotide biosynthesis (by reducing the precursor molecules such as Uridine triphosphate (UTP), Cytidine monophosphate (CMP), deoxythymidine triphosphate (dTTP), uracil, deoxyguanosine triphosphate (dGDP); tryptophan, L-methionine, and histidine biosynthesis), cell membrane disruption as well as suppression of cell wall synthesis (by inhibition of precursor molecules required for cell wall synthesis such as teichoic acid, Meso-diaminopimelate, CMP, UTP), destruction of nucleotides and intermediates such as folates that facilitate the methionine, purine, and pyrimidine biosynthesis. Nanocomposite treatment also significantly affected the osmoprotection ($P = 0.00029$) and pH-resistance ($P = 0.00039$) properties of the microbial cell. Even a significant reduction in the overall energy status of the cell due to a decrease in the energy molecules ($P = 0.00039$), lipid ($P = 0.0019$), and protein ($P \leq 0.0019$) biosynthesis has been observed. Additionally, the iron-quenching capacity is also reduced due to suppression of siderophores that lead to iron deficiency within the bacterial cell that altogether reduces the energy status of the bacterial cell. These results indicate that nanocomposite induces a holistic effect on the cellular functions (Fig. 4), not only cellular damages as reported by previous studies [30].

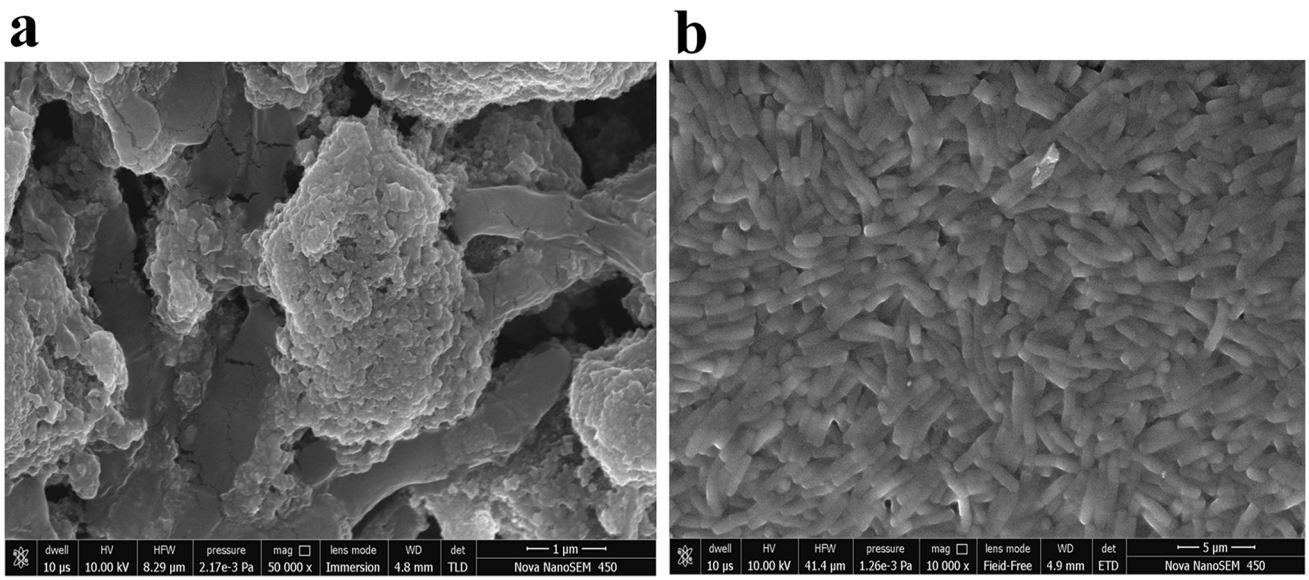

Fig. 2 Mechanism of antimicrobial action of TiO_2/CdS/ZnS nanocomposite. Nanocomposite induced changes in the cell morphology (**a**) in reference to the untreated microbial cells (**b**)

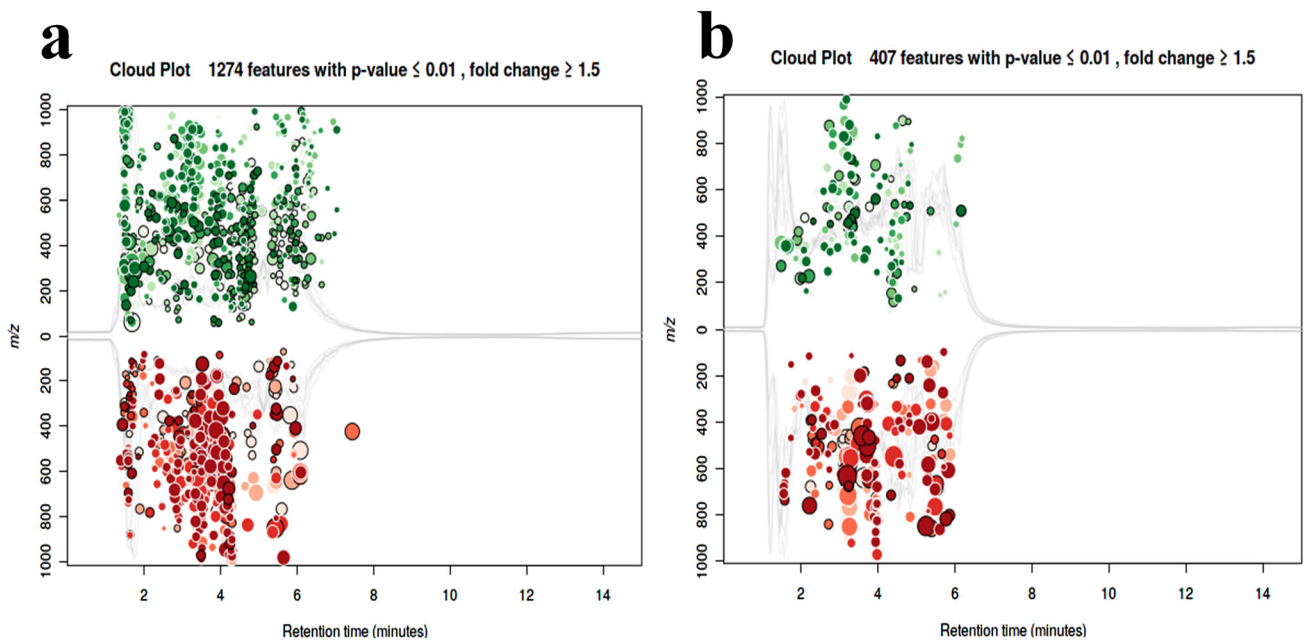

Fig. 3 Metabolomic analysis identifies statistically significant features ($P < 0.01$) after analysis of the metabolic profile captured with positive (**a**) and negative ESI mode (**b**)

Discussion

The nanomaterials can be produced through physical, chemical and biological routs with unique features such as their physical (morphology, size and particles distribution, and surface area), and chemical (composition, surface functional groups and photocatalytic activity) properties that are suitable for biotechnological application either directly or with few modifications [33–40]. TiO_2 nanocomposites are used in various therapeutic and industrial applications [25]. However, the small bandgap and limited photocatalytic activity in the visible range of the electromagnetic spectrum limit its photocatalytic activity. Efforts were made to introduce bandgap in the visible region to improve the photocatalytic activity of TiO_2 nanocomposites [26]. TiO_2 coupling with a narrow band semiconductor like CdS, Fe2O3, Cu2O, BiVO4, GaP with a bandgap of 2.4, 2.1, 2.1, 2.4, 2.3 eV respectively

Table 1 Metabolic pathways and their associated metabolic features down regulated in the microbial cell after the exposure of the nanocomposite

ESI-Mode	Metabolites	Pathway(s) involved	Fold change	*p*-value	*m/z*	Retention time	Adduct
Positive	UTP	UDP-N-acetyl-D glucosamine biosynthesis I Anhydromuropeptides recycling	204.8	2.0e-3	506.9561	4.05	M + Na[1 +]
Negative	CDP-glycerol	Teichoic acid (poly-glycerol) biosynthesis	162.8	2.6e-4	460.0502	3.59	M-H2O + H[1 +]
Negative	dTTP	Pyrimidine deoxyribonucleotide phosphorylation	125.5	1.1e-3	504.9785	3.73	M + Na[1 +]
Positive	dGDP	Guanosinedeoxyribonucleotides de novo biosynthesis I	16.0	9.6e-4	410.0251	5.96	M-H2O + H[1 +
Negative	(2S,3S)-2,3-dihydroxy-2,3-dihydrobenzoate	2,3-dihydroxybenzoate biosynthesis	15.6	5.9e-7	140.0233	5.28	M-NH3 + H[1 +]
Positive	Succinate	4-aminobutanoate degradation II	9.7	3.9e-4	136.0610	5.41	M + NH3 + H[1
Positive	CMP	Teichoic acid (poly-glycerol) biosynthesis	7.6	1.1e-4	324.0582	5.46	M + H[1 +]
Negative	Indole	L-tryptophan biosynthesis	4.2	7.1e-4	135.0918	4.59	M + NH3 + H[1 +
Positive	Meso-diaminopimelate	UDP-N-acetylmuramoylpentapeptide biosynthesis I	3.9	1.9e-3	175.1069	5.29	M-H2O + H[1 +
Positive	Histidinal	L-histidine biosynthesis	3.2	7.7e-4	82.0391	2.01	M + H + Na[2 +]
Positive	Uracil	Pyrimidine deoxyribonucleosides degradation	2.0	1.4e-4	113.0343	1.68	M + H[1 +]
Positive	N-acetyl-L-glutamate 5- semialdehyde	L-arginine biosynthesis II (acetyl cycle) L-ornithine biosynthesis I	1.7	1.9e-3	191.1022	5.89	M + NH3 + H[1

makes the composite absorb within the visible region, and the formation of heterojunctions reduces the recombination of charge carriers [27]. Further, CdS–ZnS, CdS–NiS, CdS–Cu_2O, CdS–SnS_2 binary nano-composites also absorb in the visible region and show good photocatalytic activity due to the formation of heterojunctions [28]. However, photo corrosion of these nanocomposites limits their use at a broad level. Ternary TiO_2 composites with metal oxides or sulfides in different coupling combinations not only exhibit visible absorbance and formation of heterojunctions but also reduce the photo corrosion of the catalyst [41]. In this regard, the composites of TiO_2 with other semiconductor materials are the potential candidates because they not only enhance the life span of charge carriers but also improve the absorption in the visible region [41]. In the present study, a ternary nanocomposite of TiO_2 with CdS and ZnS were synthesized. Characterization of TiO_2/CdS/ZnS nanocomposite revealed that the sample was free from impurities and highly crystalline. Even, presence of the CdS and ZnS did not affect the basic structure of the lattice. The ternary composites contain spherical nanoparticles that are well-dispersed and uniform. These results are in line with the previous studies [28].

Photo-induced antimicrobial activity of these nanocomposites needs to be assessed as the second objective of the study. The antimicrobial activity of TiO_2 nanoparticles has been reported [28–30]. Nanoparticles in general, affect the microbial electron transport, protein synthesis, nucleic acids, cell membrane, and cell wall [29, 30, 32]. Likewise, TiO_2 nanoparticles were found to attack the bacterial cell with a deteriorating effect on the cell wall, cell membrane, genetic material, transportation, communication, and respiratory processes [42]. TiO_2 induced reactive oxygen species (ROS) generation was correlated with antimicrobial activity [30]. However, the process behind TiO_2-induced ROS-based microbial death was unveiled. Additionally, microbes were characterized for the presence of cellular repair and stress tolerance machinery [43]. So, how do the nanoparticles elude these defense systems to introduce antimicrobial effects? These are a few preliminary questions that need to be addressed before describing the mechanism of antimicrobial activity.

Table 2 Metabolic pathways and their associated metabolic features upregulated in the microbial cell after the exposure of the nanocomposite

ESI-Mode	Metabolites	Pathway(s) involved	Fold change	*p*-value	*m/z*	Retention time	Adduct
Positive	(1R,6R)-6-hydroxy-2- succinylcyclohexa-2,4- diene-1-carboxylate	1,4-dihydroxy-2-naphthoate biosynthesis	13.7	2.9e-4	263.0524	4.79	M + Na[1 +]
Positive	D-mannitol 1- phosphate	Mannitol degradation I	13.7	2.9e-4	263.0524	4.79	M + H[1 +]
Positive	Palmitate	Palmitate biosynthesis II	12.1	1.4e-5	239.2366	1.73	M-H2O + H[1 +
Positive	Guanosine	Guanine and guanosine salvage	5.9	7.5e-5	306.0810	2.01	M + Na[1 +]
Negative	L-valine	L-alanine biosynthesis I	4.4	5.5e-3	119.0942	4.41	M + H[1 +]
Negative	5-aminopentanoate	L-ornithine degradation II (Stickland reaction)	4.4	5.5e-3	119.0942	4.41	M + H[1 +]
Positive	Adenosine	Adenine and adenosine salvage I	3.2	9.6e-5	290.0854	2.15	M + Na[1 +]
Positive	2'-deoxyguanosine	Purine deoxyribonucleosides degradation I	3.2	9.6e-5	290.0854	2.15	M + Na[1 +]
Positive	4-amino-4- deoxychorismate	4-aminobenzoate biosynthesis	3.1	3.6e-3	249.0606	2.50	M + Na[1 +]
Negative	3'-phosphoadenylylsulfate	Sulfate activation for sulfonation	2.8	7.7e-3	525.0204	3.27	M + NH3 + H[1 +
			2.8	9.0e-3	525.0205	2.96	M + NH3 + H[1 +
Positive	5-phospho-β-Dribosylamine	5- aminoimidazoleribonucleotide biosynthesis	2.5	1.6e-3	248.0770	1.64	M + NH3 + H[1
Positive	Protoporphyrinogen IX	Heme biosynthesis	2.2	9.3e-4	569.3127	2.68	M + H[1 +]
Positive	Pyridoxine	Pyridoxal 5'-phosphate salvage I	2.2	3.9e-3	187.1070	4.33	M + NH3 + H[1
Positive	Cytidine	UTP and CTP dephosphorylation I	2.2	1.2e-3	244.0933	4.82	M + H[1 +]
Positive	Guanine	Guanine and guanosinesalvage	2.1	3.4e-3	174.0381	2.07	M + Na[1 +]
Positive	4-aminobenzoate	4- aminobenzoatebiosynthesistetrahydrofolate biosynthesis	2.0	9.0e-4	155.0808	4.31	M + NH3 + H[1
Positive	Anthranilate	L-tryptophan biosynthesis	2.0	9.0e-4	155.0808	4.31	M + NH3 + H[1
Positive	Protoporphyrin IX	Heme biosynthesis	2.0	4.9e-3	293.1278	1.59	M + H + Na[2 +]
Negative	L-arginine	L-arginine biosynthesis II	1.5		160.1088	4.34	M-NH3 + H[1 +]

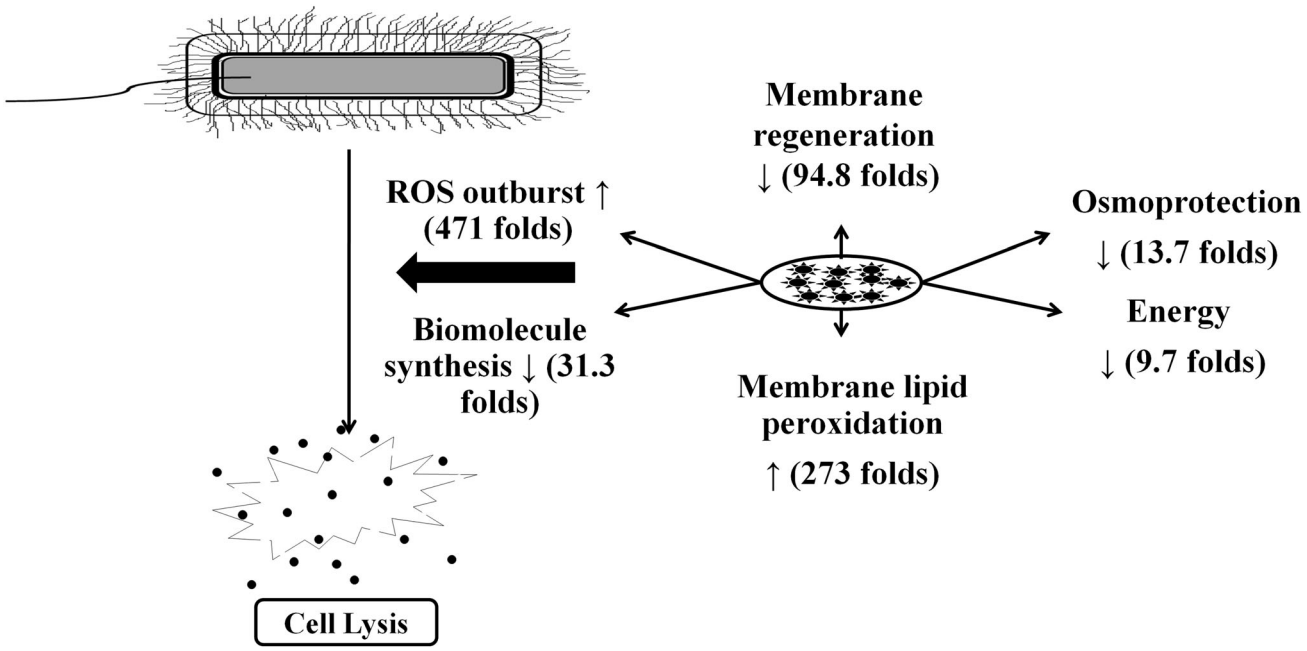

Fig. 4 Metabolomics and structural datasets described the holistic effects of the nanocomposite on the bacterial cell

Efforts are being made to decode antimicrobial mechanisms [42], however, a holistic approach is still lacking.

Photo-induced antimicrobial activity TiO_2/CdS/ZnS nanocomposite was confirmed in the current study using disc diffusion assay, time-kill kinetics, and microbroth dilution assay. Even the TiO_2/CdS/ZnS nanocomposite induced ROS generation, lipid peroxidation, and membrane disintegration was observed. These results are in line with previous studies [30] indicating ROS-based bioactivity. However, to unveil the holistic effect of the nanocomposite, additional efforts were performed to map the complete cellular metabolome using the whole-cell metabolomics approach. The cellular metabolite profile gives a precise outlook of the cellular environment [32] and is commonly employed to define the holistic influence of any external agent on cellular functioning [23, 24, 42]. Accordingly, a metabolomics approach was employed to unveil the antimicrobial mechanism of action of the nanocomposite. A total of 1681 metabolic features were differentially ($P < 0.001$) abundant among nanocomposite treated cells. These metabolites were mapped onto metabolic pathways associated with cell survivability and functioning. TiO_2/CdS/ZnS nanocomposite affects the bacterial cells similarly by influencing the vital pathways for protein, lipid, and nucleotide biosynthesis, cell membrane disruption as well as suppression of cell wall synthesis, and destruction of nucleotides and intermediates such as folates that facilitate the methionine, purine, and pyrimidine biosynthesis. Thus, the nanocomposite not only suppresses the vital microbial processes but also inhibits the repair processes. Nanocomposite treatment also significantly affects the osmoprotectant ability of the cell that in turn affects cell survivability [44]. Similarly, the osmoprotectant and pH-resistance properties of the microbial cell were affected due to the presence of TiO_2/CdS/ZnS nanocomposite. The effects on the life-sustaining processes influence microbial cell survival [45]. In the current study, the introduction of nanoparticles arrested the bacterial cell growth through inhibition of the electron transport system (by reducing the precursors that mediate the electron transfer by 9.7 folds). Disruption of electron transfer generally leads to microbial cell death [45]. A normal energy status is required for microbial cell survival [45]. A significant reduction in the overall energy status of the cell due to a decrease in the energy molecules, lipid, and protein biosynthesis has been observed similar to the observations in the previous studies [41, 42, 45]. Additionally, the iron-quenching capacity is also reduced due to suppression of siderophores that lead to iron-deficiency within the bacterial cell that altogether reduces the energy status of the bacterial cell [41, 42, 45]. These results indicate that nanocomposite induces a holistic effect on the cellular functions, not only cellular damages as reported by previous studies [30].

In this study, we prepared the ternary TiO_2 nanocomposite with a lower band gap with higher light absorption in the visible spectrum of the light. The current study also elucidated the detailed mechanism of antibacterial action of TiO_2 nanocomposite on *Bacillus subtilis*. Exposure to nanocomposite influenced microbial physiology,

metabolism, and structure (Fig. 4). These changes cumulatively affect microbial growth, repair, and maintenance that in turn lead to microbial death. Cumulatively, TiO_2/CdS/ZnS nanocomposite is a photocatalyst that embarks its potential application for the fabrication of self-sterilizing materials in various therapeutic and environment management systems.

Conflicts of interest

The authors report no conflict of interest.s

Ethics Approval

This article does not contain any studies with animals and human subjects.

Consent to Participate

All listed authors hereby submit their consent to participate.

Consent for Publication

All listed authors hereby submit their consent to publishing this study. Even there is no conflict of interest associated with this study.

Supplementary Information The online version contains supplementary material available at https://doi.org/10.1007/s12088-021-00973-z.

Acknowledgements Anuj Mittal would like to thank Council of Scientific and Industrial Research (CSIR) for fellowships.

Authors' Contributions NSC and NK designed the study. AM carried out nanocomposite synthesis and characterization, MY and TK assessed the antimicrobial properties. RC and SG performed metabolomics analysis. NSC, NK, AM, and MY performed data analysis and integration. All authors contributed to the manuscript preparation.

Funding The work was supported by grant from Principle Scientific Advisor, Government of India for the project entitled "Delhi Research Implementation and Innovation (DRIIV)".

References

1. Patel SKS, Kumar V, Mardina P, Li J, Lestari R, Kalia VC, Lee JK (2018) Methanol production from simulated biogas mixtures by co-immobilized Methylomonas methanica and Methylocella tundrae. Bioresour Technol 263:25–32. https://doi.org/10.1016/j.biortech.2018.04.096
2. Patel SKS, Lee JK, Kalia VC (2018) Beyond the theoretical yields of dark-fermentative biohydrogen. Indian J Microbiol 58:529–530. https://doi.org/10.1007/s12088-018-0759-4
3. Panday D, Patel SKS, Singh R, Kumar P, Thakur V, Chand D (2019) Solvent-tolerant acyltransferase from Bacillus sp. APB-6: purification and characterization. Indian J Microbiol 59:500–507. https://doi.org/10.1007/s12088-019-00836-8
4. Patel SKS, Ray S, Prakash J, Wee JH, Kim S-Y, Lee J-K, Kalia CV (2019) Co-digestion of biowastes to enhance biological hydrogen production by defined mixed bacterial cultures. Indian J Microbiol 59:154–160. https://doi.org/10.1007/s12088-018-00777-8
5. Lee J-K, Patel SKS, Sung BH, Kalia VC (2020) Biomolecules from municipal and food industry wastes: an overview. Bioresour Technol 298:122346. https://doi.org/10.1016/j.biortech.2029.122346
6. Patel SKS, Gupta RK, Kalia VC, Lee J-K (2021) Integrating anaerobic digestion of potato peels to methanol production by methanotrophs immobilized on banana leaves. Bioresour Technol 323:124550. https://doi.org/10.1016/j.biortech.2020.124550
7. Patel SKS, Gupta RK, Kumar V, Kondaveeti S, Kumar A, Das D, Kalia VC, Lee J-K (2020) Biomethanol production from methane by immobilized co-cultures of methanotrophs. Indian J Microbiol 60:318–324. https://doi.org/10.1007/s12088-020-00883-
8. Patel SKS, Lee JK, Kalia VC (2017) Dark-fermentative biological hydrogen production from mixed biowastes using defined mixed cultures. Indian J Microbiol 57:171–176. https://doi.org/10.1007/s12088-017-0643-7
9. Kondaveeti S, Patel SKS, Woo J, Wee JH, Kim S-Y, Al-Raoush RI, Kim I-W, Kalia VC, Lee J-K (2019) Characterization of cellobiohydrolases from Schizophyllum commune KMJ820. Indian J Microbiol 60:160–166. https://doi.org/10.1007/s12088-019-00843-9
10. Muneeswaran G, Patel SKS, Kondaveeti S, Shanmugam R, Gopinath K, Kumar V, Kim S-Y, Lee J-K, Kalia VC, Kim IW (2021) Biotin and Zn2+ increase xylitol production by Candida tropicalis. Indian J Microbiol 61:331–337. https://doi.org/10.1007/s12088-021-00960-4
11. Pagolu R, Singh R, Shanmugam R, Kondaveeti S, Patel SKS, Kalia VC, Lee J-K (2021) Site-directed lysine modification of xylanase for oriented immobilization onto silicon dioxide nanoparticles. Bioresour Technol 331:125063. https://doi.org/10.1016/j.biortech.2021.125063
12. Patel SKS, Otari SV, Li J, Kim DR, Kim SC, Cho BK, Kalia VC, Kang YC, Lee J-K (2018) Synthesis of cross-linked protein-metal hybrid nanoflowers and its application in repeated batch decolorization of synthetic dyes. J Hazard Mater 347:442–450. https://doi.org/10.1016/j.jhazmat.2018.01.003
13. Kumar V, Patel SKS, Gupta RK, Otari SV, Gao H, Lee J-K, Zhang L (2019) Enhanced saccharification and fermentation of rice straw by reducing the concentration of phenolic compounds using an immobilization enzyme cocktail. Biotechnol J 14:1800468. https://doi.org/10.1002/biot.201800468
14. Patel SKS, Choi H, Lee J-K (2019) Multi-metal based inorganic–protein hybrid system for enzyme immobilization. ACS Sustain Chem Eng 7:13633–13638. https://doi.org/10.1021/acssuschemeng.9b02583
15. Patel SKS, Gupta RK, Kumar V, Mardina P, Lestari R, Kalia VC, Choi M-S, Lee J-K (2019) Influence of metal ions on the immobilization of β-glucosidase through protein-inorganic hybrids. Indian J Microbiol 59:370–374. https://doi.org/10.1007/s12088-019-0796-z
16. Patel SKS, Gupta RK, Kim S-Y, Kim I-W, Kalia VC, Lee J-K (2021) Rhus vernicifera laccase immobilization on magnetic nanoparticles to improve stability and its potential application in bisphenol A degradation. Indian J Microbiol 61:45–54. https://doi.org/10.1007/s12088-020-00912-4

17. Kalia VC, Patel SKS, Kang YC, Lee JK (2019) Quorum sensing inhibitors as antipathogens: biotechnological applications. Biotechnol Adv 37:68–90. https://doi.org/10.1016/j.biotechadv.2018.11.006
18. Parasuraman P, Devadatha B, Sarma VV, Ranganathan S, Ampasala DR, Reddy D, Kumavath R, Kim I-W, Patel SKS, Kalia VC, Lee J-K, Siddhardha B (2020) Inhibition of microbial quorum sensing mediated virulence factors by Pestalotiopsis sydowiana. J Microbiol Biotechnol 30:571–582. https://doi.org/10.4014/jmb.1907.07030
19. Patel SK, Lee JK, Kalia VC (2020) Deploying biomolecules as anti-COVID-19 agents. Indian J Microbiol 60:263–268. https://doi.org/10.1007/s12088-020-00893-4
20. Rishi P, Thakur K, Vij S, Rishi L, Singh A, Kaur IP, Patel SKS, Lee J-K, Kalia VC (2020) Diet, Gut Microbiota and COVID-19. Indian J Microbiol 60:420–429. https://doi.org/10.1007/s12088-020-00908-0
21. Kalia VC, Patel SKS, Cho B-K, Wood TK, Lee J-K (2021) Emerging applications of bacteria as anti-tumor agents. Sem Cancer Biol. https://doi.org/10.1016/j.semcancer.2021.05.012
22. Kalia VC, Patel SKS, Shanmugam R, Lee J-K (2021) Polyhydroxy alkanoates: trends and advances towards biotechnological applications. Bioresour Technol 326:124737. https://doi.org/10.1016/j.biortech.2021.124737
23. Patel SKS, Kim J-H, Kalia VC, Lee J-K (2019) Antimicrobial activity of aminoderivatized cationic polysaccharides. Indian J Microbiol 59:96–99. https://doi.org/10.1007/s12088-018-00764-7
24. Otari SV, Pawar SH, Patel SKS, Singh RK, Kim S-Y, Lee J-H, Zhang L, Lee J-K (2017) Canna edulis leaf extract-mediated preparation of stabilized silver nanoparticles: characterization, antimicrobial activity, and toxicity studies. J Microbiol Biotechnol 27:731–738. https://doi.org/10.4014/jmb.1610.10019
25. Wanag A, Rokicka P, Kusiak-Nejman E, Kapica-Kozar J, Wrobel RJ, Markowska-Szczupak A, Morawski AW (2018) Antibacterial properties of TiO2 modified with reduced graphene oxide. Ecotoxicol Environ Saf 147:788–793. https://doi.org/10.1016/j.ecoenv.2017.09.039
26. Kumar N, Chauhan NS, Mittal A, Sharma S (2018) TiO_2 and its composites as promising biomaterials: a review. Biometals 31(2):147–159. https://doi.org/10.1007/s10534-018-0078-6
27. Ziental D, Czarczynska-Goslinska B, Mlynarczyk DT, Glowacka-Sobotta A, Stanisz B, Goslinski T, Sobotta L (2020) Titanium dioxide nanoparticles: prospects and applications in medicine. Nanomaterials (Basel) 10(2):387. https://doi.org/10.3390/nano10020387
28. Mittal A, Sharma S, Kumari V, Yadav S, Chauhan NS, Kumar N (2019) Highly efficient, visible active TiO_2/CdS/ZnS photocatalyst, study of activity in an ultra low energy consumption LED based photo reactor. J Mater Sci: Mater Electron 30:17933–17946. https://doi.org/10.1007/s10854-019-02147-6
29. Ranjan S, Ramalingam C (2016) Titanium dioxide nanoparticles induce bacterial membrane rupture by reactive oxygen species generation. Environ Chem Lett 14:487–494. https://doi.org/10.1007/s10311-016-0586-y
30. Planchon M, Léger T, Spalla O, Huber G, Ferrari R (2017) Metabolomic and proteomic investigations of impacts of titanium dioxide nanoparticles on *Escherichia coli*. PLoS ONE 12(6):e0178437. https://doi.org/10.1371/journal.pone.0178437
31. Dong Y, Zhu H, Shen Y, Zhang W, Zhang L (2019) Antibacterial activity of silver nanoparticles of different particle size against *Vibrio natriegens*. PLoS ONE 14(9):e0222322. https://doi.org/10.1371/journal.pone.0222322
32. Zhang A, Sun H, Xu H, Qiu S, Wang X (2013) Cell metabolomics. OMICS 17(10):495–501. https://doi.org/10.1089/omi.2012.0090
33. Patel SKS, Choi SH, Kang YC, Lee J-K (2016) Large-scale aerosol-assisted synthesis of biofriendly Fe2O3 yolk-shell particles: a promising support for enzyme immobilization. Nanoscale 8:6728–6738. https://doi.org/10.1039/C6NR00346J
34. Patel SKS, Choi SH, Kang YC, Lee J-K (2017) Eco-friendly composite of Fe3O4-reduced graphene oxide particles for efficient enzyme immobilization. ACS Appl Mater Interfaces 9:2213–2222. https://doi.org/10.1021/acsami.6b05165
35. Patel SKS, Anwar MZ, Kumar A, Otari SV, Pagolu R, Kim SY, Kim IW, Lee J-K (2018) Fe2O3 yolk-shell particles-based laccase biosensor for efficient detection of 2,6-dimethoxyphenol. Biochem Eng J 132:1–8. https://doi.org/10.1016/j.bej.2017.12.013
36. Otari SV, Patel SKS, Kim S-Y, Haw JR, Kalia VC, Kim I-W, Lee J-K (2019) Copper ferrite magnetic nanoparticles for the immobilization of enzyme. Indian J Microbiol 59:105–108. https://doi.org/10.1007/s12088-018-0768-3
37. Otari SV, Shinde VV, Gao H, Patel SKS, Kalia VC, Kim IW, Lee JK (2019) Biomolecule entrapped SiO2 nanoparticles for ultrafast green synthesis of silver nanoparticle-decorated hybrid nanostructures as effective catalyst. Ceram Int 45:5876–5882. https://doi.org/10.1016/j.ceramint.2018.12.054
38. Patel SKS, Jeon MS, Gupta RK, Jeon Y, Kalia VC, Kim SC, Cho BK, Kim DR, Lee J-K (2019) Hierarchical macro-porous particles for efficient whole-cell immobilization: application in bioconversion of greenhouse gases to methanol. ACS Appl Mater Interfaces 11:18968–18977. https://doi.org/10.1021/acsami.9b03420
39. Kumar A, Park GD, Patel SKS, Kondaveeti S, Otari S, Anwar MZ, Kalia VC, Singh Y, Kim SC, Cho B-K, Sohn J-H, Kim DR, Kang YC, Lee J-K (2019) SiO2 microparticles with carbon nanotube-derived mesopores as an efficient support for enzyme immobilization. Chem Eng J 359:1252–1264. https://doi.org/10.1016/j.cej.2018.11.052
40. Otari SV, Patel SKS, Kalia VC, Lee J-K (2020) One-step hydrothermal synthesis of magnetic rice straw for effective lipase immobilization and its application in esterification reaction. Bioresour Technol 302:122887. https://doi.org/10.1016/j.biortech.2020.122887
41. Wu K, Wu P, Zhu J, Liu C, Dong X, Wu J, Meng G, Xu K, Hou J, Liu Z, Guo X (2019) Synthesis of hollow core-shell CdS@TiO_2/Ni_2P photocatalyst for enhancing hydrogen evolution and degradation of MB. Chem Eng J 360:221–230. https://doi.org/10.1016/j.cej.2018.11.211
42. Azizi-Lalabadi M, Ehsani A, Divband B, Alizadeh-Sani M (2010) Antimicrobial activity of Titanium dioxide and Zinc oxide nanoparticles supported in 4A zeolite and evaluation the morphological characteristic. Sci Rep 9:17439. https://doi.org/10.1038/s41598-019-54025-0
43. Ahmed V, Verma MK, Gupta S, Mandhan V, Chauhan NS (2018) Metagenomic profiling of soil microbes to mine salt stress tolerance genes. Front Microbiol 9:159. https://doi.org/10.3389/fmicb.2018.00159
44. Hong Y, Zeng J, Wang X, Drlica K, Zhao X (2019) Post-stress bacterial cell death mediated by reactive oxygen species. Proc Natl Acad Sci USA 116:10064–10071. https://doi.org/10.1073/pnas.1901730116
45. Rice KC, Bayles KW (2008) Molecular control of bacterial death and lysis. Microbiol Mol Biol Rev 72(1):85–109. https://doi.org/10.1128/MMBR.00030-07